Major Category: BIOLOGICAL SCIENCES

Minor Category: Biophysics and Computational Biology

Role of Boundary Conditions in Determining Cell Alignment in Response to Stretch

Kellen Chen[1], Andrea Vigliotti[3], Mattia Bacca[4,5], Robert M. McMeeking[4,5], Vikram S. Deshpande[3], Jeffrey W. Holmes[1,2]

Departments of [1]Biomedical Engineering and [2]Medicine, University of Virginia, Charlottesville, VA 22908; [3]Department of Engineering, University of Cambridge, Trumpington Street, Cambridge CB2 1PZ, United Kingdom; Departments of [4]Mechanical Engineering and [5]Materials, University of California, Santa Barbara, Santa Barbara, CA 93106

Corresponding Author: Jeffrey W. Holmes, M.D., Ph.D.

Department of Biomedical Engineering

Box 800759, University of Virginia

Charlottesville, Virginia 22908

434-243-6321 / holmes@virginia.edu

Keywords: cell mechanics, cytoskeleton, stress fibers, computational modeling, fibroblasts, cell orientation

Abstract

The ability of cells to orient in response to mechanical stimuli is essential to embryonic development, cell migration, mechanotransduction, and other critical physiologic functions in a range of organs. Endothelial cells, fibroblasts, mesenchymal stem cells, and osteoblasts all orient perpendicular to an applied cyclic stretch when plated on stretchable elastic substrates, suggesting a common underlying mechanism. Yet many of these same cells orient parallel to stretch in vivo and in 3D culture, and a compelling explanation for the different orientation responses in 2D and 3D has remained elusive. Here, we employed a novel experimental system to conduct a series of experiments designed specifically to test the hypothesis that differences in strains transverse to the primary loading direction give rise to the different alignment patterns observed in 2D and 3D cyclic stretch experiments ("strain avoidance"). We found that in static or low-frequency stretch conditions, cell alignment in fibroblast-populated collagen gels correlated with the presence or absence of a restraining boundary condition, rather than with compaction strains. Cyclic stretch could induce perpendicular alignment in 3D culture, but only at frequencies an order of magnitude greater than reported to induce perpendicular alignment in 2D. We modified a published model of stress fiber dynamics and were able to reproduce our experimental findings across all conditions tested, as well as published data from 2D cyclic stretch experiments. These experimental and model results suggest a new explanation for the apparently contradictory alignment responses of cells subjected to cyclic stretch on 2D membranes and in 3D gels.

Significance Statement

Alignment of cells in response to mechanical cues plays an important role in a wide range of physiologic processes. Multiple cell types orient perpendicular to applied cyclic stretch in 2D culture but parallel to stretch in 3D culture, and the mechanisms underlying this behavior remain elusive. We tested a promising hypothesized mechanism called strain avoidance and showed that it cannot explain cell alignment across the conditions we examined. By contrast, a computational model of stress fiber kinetics incorporating the influence of traction boundary conditions and altered strain transmission in soft gels reproduced all of our experimental results as well as published 2D stretch experiments. These findings could improve understanding, modeling, and therapeutic modulation of tissue development, regeneration, and repair.

\body

Introduction

Alignment of cells in response to mechanical cues plays an important role in a wide range of physiologic responses, from sensing of shear stress by endothelial cells to production of aligned collagen in developing tendons. One of the most intriguing observations to emerge from studying these responses is that cells plated on a flexible 2D substrate orient perpendicular to an applied uniaxial cyclic stretch (1–6), while cells embedded in a 3D gel orient parallel to that stretch (7–13). Recently, Obbink-Huizer et al. (14) proposed an attractive hypothesis to explain this discrepancy. They postulated that the dominant cellular response in both situations is strain avoidance, in which net disassembly of stress fibers parallel to an applied strain produces cytoskeletal alignment perpendicular to that strain. According to this hypothesis, cells in 3D gels align parallel to applied cyclic stretch because they are able to compact these gels perpendicular to the stretch direction, producing compaction strains that are much larger than the applied cyclic strains; in other words, cells in gels align with applied stretch only because they are avoiding much larger transverse compaction strains.

To date, only limited experimental data are available to assess this hypothesis. Foolen et al. (8) designed a collagen gel loading system that allowed them to perform either uniaxial cyclic stretching (in the x_1 direction with x_2 left free to compact) or strip uniaxial cyclic stretching (in the x_1 direction with x_2 constrained). However, this experimental system simultaneously varied both compaction and boundary conditions in the x_2 direction. In order to specifically test the hypothesis that transverse compaction explains cell alignment parallel to stretch in 3D culture, we developed a system that

allowed us to independently control compaction in the loading and transverse directions, prior to and during the application of cyclic uniaxial stretch. Experiments with this new system suggested that traction boundary conditions – rather than compaction per se – govern the alignment of cardiac fibroblasts cultured in statically restrained collagen gels. Cyclic uniaxial stretch could modify this alignment, but only at frequencies an order of magnitude greater than required to induce perpendicular alignment in published 2D stretching experiments. We then modified a thermodynamic model of stress fiber dynamics published recently by Vigliotti et al. (15) and were able to reproduce these new experimental findings as well as previously published data from 2D cyclic stretching experiments. These experiments and model results suggest a new framework for understanding the apparently contradictory alignment responses of cells subjected to cyclic stretch on 2D membranes and in 3D gels.

Results and Discussion

Cellular Alignment in the Presence of Transverse Compaction

In order to separate the effects of compaction and boundary conditions, we subjected collagen gels containing primary adult cardiac fibroblasts to different combinations of experimental conditions during a 24h pre-culture period and subsequent cyclic stretch periods (Fig. 1). In one group, we restrained gels during pre-culture, then left the x_2 direction free while we imposed low-frequency uniaxial stretch (10%, 0.5 Hz) or restraint (0% stretch) in the x_1 direction (Fig. 1C). Marker-based measurements of deformation in the central region of these gels confirmed the

presence of substantial transverse compaction (Fig. 2B). Fibroblasts were randomly aligned after the pre-culture phase, but aligned strongly in the x_1 direction (parallel to stretch) during the stretching phase (Fig. 2C, Fig. 3A,B). This experiment replicates the classic 3D results described previously by multiple groups, wherein cells in 3D culture align parallel to an imposed stretch (7, 8, 16). Unfortunately, this experiment alone provides limited insight into the factors governing cell alignment because so many potential determinants co-vary. Cells could be aligning parallel to the imposed stretch or restraint or perpendicular to the compaction strains; furthermore, since transverse compaction generates collagen alignment parallel to a uniaxial restraint (7, 11, 16, 17), cells could also be aligning along the local collagen fiber direction.

Cellular Alignment in the Presence of Isotropic Compaction

In order to better separate these potentially confounding variables, we took advantage of the fact that collagen gel compaction is very rapid during the first few hours, then slows dramatically (Fig. 1E) (18). Thus, when we left gels unconstrained in both directions for 24 hours, they compacted isotropically, inducing no net cell alignment (Fig. 2D,E,F). 24 hours of subsequent uniaxial restraint or low-frequency cyclic stretch (10%, 0.5 Hz) along the x_1 direction produced no additional transverse compaction in the x_2 direction, yet cells aligned strongly over that same time period; thus it seems clear that compaction strains could not be the primary driver of cell alignment in this experiment. We note that with longer culture periods in this experimental group, we did see some additional x_2 compaction. However, this compaction was not associated with higher levels of cell alignment (Fig. 2D,E,F, Fig. 3D,E), again demonstrating a lack of

correlation between the degree of transverse compaction and the degree of cell alignment.

Cellular Alignment in the Absence of Compaction

In other gels, we prevented transverse compaction by constraining gels biaxially during the pre-culture period and then applying "strip uniaxial" stretch conditions: stretching (10%, 0.5 Hz) or restraining (0% stretch) gels in the x_1 direction while preventing deformation in the x_2 direction (Fig. 1D). As expected, these gels displayed no transverse compaction (Fig. 2H). According to the strain avoidance hypothesis, this experiment should produce similar results to those observed with cells cultured on 2D stretchable membranes: in the absence of transverse compaction, cells should avoid the imposed 10% cyclic strain and orient perpendicular to the loading direction. In contrast to this expectation, we found that average fibroblast alignment remained low at all time points in these gels (Fig. 2I), and histograms showed similar numbers of cells oriented in all directions (Fig. 3G,H).

These results are consistent with most previous reports employing 3D gels, but there are some inconsistencies. In agreement with our findings, Foolen et al. (8) reported that vascular-derived cells cultured in collagen/matrigel gels developed random orientations during an initial biaxial constraint and that subsequent 10% strip uniaxial cyclic stretch at 0.5 Hz caused no change in the orientation within the core of the gel. However, they also reported that cells on the top and bottom surfaces of their gels aligned perpendicular to the direction of stretch (8); by contrast, cells at the surface and within the core of our gels showed similar alignment responses in all conditions. In

another study, De Jonge et al. (19) reported that myofibroblasts and collagen in 3D fibrin gels subjected to 5% strip uniaxial cyclic stretch at 1 Hz oriented perpendicular to the stretch direction, which appears to contradict both our data and that of Foolen.

Effect of Stretching Frequency on Cellular Alignment in 3D Gels

Published data suggest that cells on 2D elastic membranes subjected to cyclic uniaxial stretch align perpendicular to stretch only above a critical frequency of approximately 0.1 Hz (20–22). We therefore tested the possibility that higher frequencies might induce perpendicular alignment in our strip uniaxial gels; for comparison we imposed the same stretch conditions on uniaxially stretched gels. We plotted an order parameter that quantifies alignment (1 = parallel, -1 = perpendicular, 0 = random, see equation (5) in Materials and Methods) as a function of frequency alongside published 2D data (22) from cyclically stretched rat embryonic fibroblasts (Fig. 4A). Cells in gels subjected to strip uniaxial stretch showed no alignment at 0.5 Hz, modest but statistically significant perpendicular alignment at 2 Hz, and clear perpendicular alignment at 4 Hz (orientation histograms for each case provided in the SI Appendix, Fig. S2). Thus, under strip uniaxial conditions it was possible to induce perpendicular alignment similar to that commonly observed in 2D, but the transition frequency at which this occurred was an order of magnitude higher in our gel experiments than has been reported in 2D. Cells in gels subjected to uniaxial stretch with the x_2 direction left free showed clear parallel alignment at 0.5 Hz, modest but statistically significant alignment at 2 Hz, and no significant alignment at 4 Hz (Figs. 4A, S2).

Mechanical Determinants of Cell Alignment in 2D and 3D

Our experimental results suggest thinking about the mechanical factors that influence cell alignment on two different time scales. On the time scale of individual stretch and release cycles, sufficiently rapid or large strains do appear to modify cell alignment in 3D, inducing perpendicular alignment under conditions where static culture would produce randomly oriented cells and reducing parallel alignment under conditions where static culture would produce it. These observations are generally consistent with previous models (14, 23) in which high strain rates either reduce stress fiber assembly or promote disassembly. However, any model that aims to simultaneously capture both 2D and 3D responses must explain why the transition frequency for perpendicular alignment appears to differ in these settings (Fig. 4A). We have incorporated one hypothesis to explain this discrepancy in the computational model presented below.

On the time scale of hours to days over which compaction of 3D gels occurs, we found that strain avoidance could not explain the alignment responses we observed. When cultured statically or at frequencies too low to induce reorientation, cells in gels restrained in the x_1 direction aligned just as strongly whether they compacted only in the x_2 direction or equally in both directions (Figs. 2, 3). Thus, we believe the data presented here support the alternate hypothesis that cell alignment in these experiments was primarily determined by the presence or absence of a restraining boundary condition. This alternate hypothesis fits better with prior observations that cells in collagen gels actively remodel the surrounding collagen as well as their attachments to it on a timescale of hours to days, making it difficult to imagine how cells

would “remember” compaction strains over these longer times. The boundary condition hypothesis would also be consistent with a prior study by Lee et al., who allowed cell and collagen alignment to develop in uniaxially restrained collagen gels, then switched the direction of restraint from x_1 to x_2 (7). Following the switch, cells re-oriented rapidly into the new direction of restraint (and away from the dominant collagen fiber direction), then gradually began reorienting collagen fibers towards the new preferred cell direction. This result suggested that the cells could sense and respond to a change in the direction of restraint independently of the alignment cues provided by surrounding collagen fibers, but did not directly address the role of compaction strains vs. restraint.

Computational Predictions of Cell Alignment

In order to explore potential mechanisms that might explain the experimental results reported here, we modified a previously published model by Vigliotti et al. (15) that predicts the steady-state distribution of stress fibers (SFs) by accounting for the effects of imposed stretch and shortening on the kinetics of SF assembly and disassembly. The equations and details of the modified model are presented in the SI Appendix, but conceptually we made two modifications that reflect our proposed explanations for the novel findings presented above.

Our first modification to the original Vigliotti model was to assume that cells can remodel the surrounding collagen, their attachments to that collagen, and their cytoskeleton over time scales much longer than an individual loading cycle to achieve a state at which the increase in elastic energy due to stretching the cell beyond its reference configuration was balanced by the decrease in cytoskeletal free energy due to

SF assembly (SI Appendix, Fig. S1). As noted above, there is ample experimental evidence that cells embedded in collagen gels do remodel the surrounding collagen and their attachments (24–26), but the hypothesis that this remodeling minimizes the free energy of the cell remains to be tested. When both the x_1 and x_2 directions were restrained as in our strip uniaxial stretching experiments, cells reached this minimum-energy state at stretches $F_{11} = 1.062$, $F_{22} = 1.062$ (SI Appendix, Fig. S1A). By contrast, when the x_1 direction was constrained and the x_2 direction left free as in our uniaxial stretching experiments, cells reached equilibrium at stretches $F_{11} = 1.075$, $F_{22} = 0.7893$ (SI Appendix, Fig. S1B,C). Importantly, these stretches depended on the presence/absence of restraint in each direction, but not on the compaction history, because the cells in the model respond to compaction or stretch by shortening or lengthening individual SFs to hold the strain in each actomyosin subunit constant. Integrating these equilibrium stretches into the Vigliotti model resulted in nearly isotropic predicted stress fiber distributions for strip uniaxial stimulations of static and low-frequency stretch conditions (Fig. 3I). By contrast, in all uniaxial simulations where the x_2 boundary of the gels was left free, the model predicted strong SF alignment in the x_1 direction (Fig. 3C,F), consistent with the experimentally measured cell orientation distributions.

Our second modification accounts for the fact that when cells are embedded in very soft gels, the cells and gel act as springs in series, and the cells experience only a fraction of the stretch applied globally to the gel (27). In the Vigliotti model, large negative strain rates lead to lower SF forces due to the force-velocity behavior of

myosin, discouraging parallel assembly and encouraging perpendicular assembly. Assuming that cells experience all of the global applied stretch in 2D but only a fraction of that stretch in a soft 3D gel, the model predicted that higher frequencies (or higher stretches) are required to modify SF distributions in 3D vs. 2D, in agreement with our 3D experiments and published 2D data (Fig. 4B; orientation histograms for 3D simulations provided in the SI Appendix, Fig. S2D,H). Together, these two modifications to the Vigliotti model allowed it to correctly predict not only the classic frequency-dependent perpendicular orientation response for 2D cyclic stretch experiments but also all of the key alignment responses reported here: 1) Under uniaxial restraint, cells in gels align parallel to the restraint regardless of the degree of transverse compaction; 2) Superimposing uniaxial cyclic stretch decreases the strength of that alignment in a frequency-dependent manner; 3) Under biaxial restraint, cells in gels align randomly; and 4) Superimposing uniaxial cyclic stretch promotes perpendicular alignment in a frequency-dependent manner.

A number of published models have addressed the effects of mechanical stretch on cell orientation (14, 15, 23, 28, 29). Several of these are conceptually similar: they use a set of differential equations to track the assembly and disassembly of SF families or subsets oriented in different directions and then introduce experimentally-motivated phenomenologic terms that modify the assembly or disassembly rates. For example, Kaunas and Hsu assumed that stretch or shortening of a SF relative to its preferred homeostatic length promotes disassembly (28); in this model, cyclic stretching induces cell alignment perpendicular to the stretch direction by forcing SF disassembly in that

direction. Desphande et al. assumed that stress within the SFs reduces the disassembly rate, so that cells develop more SFs on stiffer substrates and along the local direction of greatest resistance to cell contraction (23); in their model, uniaxial cyclic stretch reduces stress in SFs parallel to the stretch direction through the force-velocity behavior of the actomyosin subunits, resulting in disassembly of parallel SFs and net cell orientation perpendicular to the stretch. Obbink-Huizer et al. constructed a similar model, but assumed that higher SF tension promotes SF assembly rather than inhibiting disassembly. They included not only force-velocity but also force-length behavior of the SFs, such that active stress generation by the SFs decreased with either stretch or shortening (14); as a consequence, cells in their model turn perpendicular to an applied cyclic stretch or to a cell-induced compaction strain, with the larger strain dominating when both are present. The Vigliotti model employed here incorporates some of the key components of previous models (such as force-length and force-velocity behavior of actomyosin) into a thermodynamically motivated framework, in which stresses or deformations influence SF assembly by altering the free energy of bound actomyosin subunits (15).

All of these models capture the experimental observation that cells on 2D substrates align parallel to a static restraint but perpendicular to an applied uniaxial cyclic stretch. Adding our assumption that only a fraction of the globally applied stretch is transferred to cells in soft gels would likely allow several of these models to also capture the difference in transition frequency between 2D and 3D experiments (Fig. 4). Of these models, only the Obbink-Huizer and Vigliotti models correctly predict that cells

embedded in a 3D gel align parallel to uniaxial cyclic stretch, but both models rely on the magnitude of transverse compaction strains to make this prediction. In the Obbink-Huizer model, compaction strains perpendicular to the stretch direction reduce perpendicular SF assembly much more than the cyclic stretching reduces parallel SF assembly. In the Vigliotti model, SFs rapidly add or subtract actomyosin subunits along their length to hold the strain on individual subunits constant; large compaction strains perpendicular to stretch produce very short SFs in that direction, which are thermodynamically less stable than the longer SFs that persist in the stretch direction. Based on the new experimental data presented here, our revised model proposes a slightly different mechanism: in the absence of external restraint, the minimum-energy equilibrium state for a cell embedded in a soft gel is one with very short, unstable SFs, while in the presence of restraint, equilibrium is achieved with longer, more stable SFs. In the presence of anisotropic boundary conditions, the SFs in different directions achieve a mix of these states, and perturbations due to cyclic stretch are then superimposed on this basal state. One conceptual advantage of this mechanism is that it does not assume that cells “remember” compaction strains that may have occurred days or weeks earlier, or even that changes induced in the cytoskeleton by compaction are maintained over long times; rather, it assumes only that the cell will continually remodel its cytoskeleton, surrounding ECM, and/or connections to that ECM to seek a minimum-energy state.

Limitations and Sources of Error

Most models of the effects of stretch on cell orientation (including the one employed here) predict distributions of stress fibers within a single hypothetical cell. However, most experiments quantify the alignment of many cells subjected to a given experimental condition, in order to account for biologic variability and stochasticity that may not be represented in models. Thus, we do not expect model-predicted SF distributions to precisely match experimentally measured cell orientation distributions (Figs. 3, S2). Instead, we focused on features such as mean orientation and strength of alignment that we expected to be more comparable. To test whether these features are in fact comparable between stress fiber (SF) and cell orientation distributions, we measured SF and cell orientations in the same subset of cells. The mean orientation computed from stress fibers within each cell (mean angle, MA^{SF}) correlated almost 1:1 with the alignment of that same cell computed from the cell boundary (MA^{cell}), increasing our confidence in comparisons between model-predicted mean stress fiber orientation and experimentally measured mean cell orientation (SI Appendix, Fig. S3A). The strength of alignment computed from analyzing stress fibers (mean vector length, MVL^{SF}) also correlated with but was consistently lower than that computed from the cell boundary (MVL^{cell}) (SI Appendix, Fig. S3B). On a cell-by-cell basis, this observation reflects the fact that even in cells that were clearly spindle-shaped and strongly aligned in a preferred direction, we frequently observed individual stress fibers oriented away from the primary cell axis.

Limitations of the computational model presented here include the fact that we validated its predictions of cell alignment responses against experimental results for cyclic stretch at a range of frequencies from 0-4 Hz and amplitudes ranging from 0-10%, but predictions for other frequencies and amplitudes remain to be validated. In addition, although we expect that collagen gels that compacted more in the x_2 than in the x_1 direction in our experiments also developed some degree of collagen fiber alignment along the x_1 axis, we did not measure those collagen orientations or include them in our computational model of cell alignment. Our primary justification for this omission is that our prior studies have clearly shown that isotropic compaction maintains random collagen orientation in the x_1-x_2 plane in these gels (11), yet some of our gels developed very strong cell alignment in the presence of isotropic compaction strains (i.e., 24h group in Fig. 2D,E,F). Thus, while contact guidance is certainly an important alignment cue in many settings, in our experiments it does not appear to be the dominant mechanism underlying cell alignment. Finally, the free-energy minimization approach used here to compute the equilibrium strain state of simulated cells ignored exchange of nutrients and heat with the surrounding bath and neglected the entropy and distribution of states observed in actual cell populations.

Materials and Methods

Fabrication and Loading of Fibroblast-Populated Collagen Gels

We isolated and cultured adult rat cardiac fibroblasts and generated fibroblast-populated collagen hydrogels as previously published (17, 30); details are provided in

the SI Appendix. Gels containing a final concentration of 200k cells/mL and 2 mg/mL collagen were polymerized and constrained in both directions or left to compact isotropically during a 24h pre-culture period before transfer to the loading system (Fig. 1A). We used CellScale MechanoCulture B1 devices (CellScale, Waterloo, ON, Canada) to either statically or dynamically load the cell-populated collagen hydrogels (Fig. 1B). These devices included a “dry” side, housing a circuit board and motor that could be programmed for a variety of amplitudes or frequencies of stretch (right side of Fig. 1B), connected by a stainless steel bridge to a “wet” side filled with 10% FBS containing media. Three interconnected deformable polyether ether ketone (PEEK) plastic layers transferred linear motion of the bridge into stretch of an inner circle (3.6cm diameter) of 24 pins. We pinned the arms of the collagen gels in the x_1 direction, and either pinned the arms in the x_2 direction to prevent compaction (strip uniaxial stretch) or cut them off to allow compaction (uniaxial stretch).

We transferred gels initially cultured under biaxial constraint to the B1 devices and subjected them to either 0% uniaxial stretch (x_1 direction constrained, x_2 direction left free to compact), 10% cyclic uniaxial stretch (stretch applied in the x_1 direction, x_2 direction left free to compact) (Fig. 1C), 0% strip uniaxial stretch (both directions constrained), or 10% cyclic strip uniaxial stretch (stretch applied in the x_1 direction, x_2 direction held fixed) (Fig. 1D). In this paper, we use “0% strip uniaxial stretch” and “0% uniaxial stretch” (synonymous to a biaxial and uniaxial constraint, respectively) in order to differentiate these loading conditions in the stretcher from the pre-culture conditions. We also transferred the gels that initially floated freely in media and compacted

isotropically to CellScale devices and subjected them to either 0% uniaxial stretch or 10% cyclic uniaxial stretch (Fig. 1E). We mapped the time course of the static (0%) and low-frequency (10%, 0.5 Hz) responses using 15 gels for each of these six conditions: five stretched for 24 h, five for 48 h, and five for 72 h. We explored the effect of higher frequencies by stretching gels for 72 h under each of the following conditions: 10% cyclic uniaxial stretch at 2 Hz (n=5), 10% cyclic uniaxial stretch at 4 Hz (n=4), 10% cyclic strip uniaxial stretch at 2 Hz (n=5), and 10% strip cyclic uniaxial stretch at 4 Hz (n=5). The five gels in any one experimental group contained cells from five separate rat fibroblast isolations. In addition to the 109 gels listed above, eight gels underwent the initial pre-culture step only (n=4 biaxial constraint, n=4 isotropic compaction).

Quantification of gel compaction

We applied nine titanium oxide paint dots, consisting of 1 g/mL Titanium(IV) oxide powder (Sigma-Aldrich) mixed with PBS, on the surface of the central region of the gel (box in Fig. 1A) with a 7-0 nylon suture (Ethicon, 1647G) and used these markers to track compaction over the course of the experiment. We used a digital camera to image the markers before the pre-culture period, after the pre-culture period prior to the onset of loading, and at the end of each loading protocol. All images were taken when the stretching devices were at the 0% strain position, so marker positions in these images reflected the deformations due to gel compaction. We used the markers to compute a single homogeneous deformation gradient tensor **F** that provided the least-squares best fit mapping of the 9 marker positions from the undeformed

(beginning of experiment) to deformed positions by solving the overdetermined matrix equation:

$$\boldsymbol{x} = \boldsymbol{FX} + \boldsymbol{p} \quad (1),$$

where **p** is an arbitrary vector included to account for translation between images.

Microscopy and quantification of cell alignment

After the stretch protocols, we fixed the gels in 10% formalin, stained the F-actin with Alexa Fluor 488 Phalloidin (Thermo Fisher Scientific, A12379), and used a confocal microscope with a 10x objective to capture z-stacks consisting of one image every 2.5μm through the gel thickness at three locations in the central region. Within each z-stack, we created 2D projections (SI Appendix, Fig. S4A) by combining sets of 10 consecutive images separated by 25 μm, allowing for analysis of non-overlapping cells at different depths below the gel surface. Using MATLAB, we converted each 2D projection to binary (fluorescent pixels = white, dark pixels = black) and analyzed white pixel clusters above a size threshold of 15μm x 15μm (SI Appendix, Fig. S4B).

We tracked the orientation and strength of alignment of fibroblasts using mean vectors calculated using equations 2-4, consistent with circular statistics theory for the analysis of angular data (31):

$$Y = \frac{\sum\left(L_j * \sin(2\theta_j)\right)}{N} \qquad \mathrm{X} = \frac{\sum(L_j * \cos(2\theta_j))}{N} \quad (2)$$

$$MVL = \sqrt{(Y)^2 + (X)^2} \quad (3)$$

$$MA = \frac{1}{2}\arctan\left(\frac{Y}{\mathrm{X}}\right) \quad (4)$$

For each cell, we constructed 400 vectors from the centroid to equally spaced points around the cell boundary. We used the lengths and angles of these vectors (L_j and θ_j, with j = 1,2,…N and N = 400) to compute a vector whose length, MVL^{cell}, indicated strength of alignment (ranging from $MVL^{cell} = 0$ for a circular cell to $MVL^{cell} = 1$ for a highly aligned, spindly cell), and mean angle, MA^{cell} indicated orientation (SI Appendix, Fig. S4C). The 2θ terms in equations 2 and ½ term in equation 4 account for the fact that the full range of possible angles is only 180°, since a cell oriented horizontally could be correctly described as oriented at 0° or at 180° (31). We then combined the individual cell vectors for all cells in each gel and used equations 2-4 to compute a mean vector that reflected the mean strength of cell alignment within each gel (MVL^{gel}, ranging from $MVL^{gel} = 0$, all cells aligned randomly, to $MVL^{gel} = 1$, all cells aligned in the same direction) and direction (MA^{gel}) for the entire gel (SI Appendix, Fig S4D). Finally, we averaged MVL^{gel} values across the (n=5) gels for each experimental condition.

Quantification of Parallel vs. Perpendicular Alignment of Cells and SFs

In order to quantitatively compare the alignment and directionality of experimentally measured cells and computationally simulated SFs at different frequencies, we used an order parameter (21, 22):

$$S = < cos2\theta > = \int h(\theta) \cos(2\theta) d\theta, \quad (5)$$

where $h(\theta)$ represents the probability distribution histogram of cells or SFs in each angular bin. S ranges from S = 1, all cells or stress fibers aligned completely parallel to the stretch (x_1) direction, to S = -1, all cells or fibers aligned completely perpendicular to stretch, with S = 0 representing completely random alignment.

Experimental Measurements of Cell Alignment in 2D

Jungbauer et al. (22) explored the effects of various stretch amplitudes and frequencies on cells cultured on top of 2D silicone elastomer membranes and used the same $S=\langle\cos 2\theta\rangle$ order parameter (equation 5) to measure cell alignment. We digitized their figures for rat embryonic fibroblasts subjected to 30 x 10^3 s (8.33 h) of 8% uniaxial cyclic stretch at 0.01, 0.25, 2, and 15 Hz to obtain their mean $\pm$ SD alignment values for 30-50 cells per tested frequency.

Statistics

We used a two-way ANOVA to assess whether transverse compaction (F_{22}) or alignment (MVL) varied significantly across the stretch amplitudes (0%, 10% 0.5 Hz) and durations (24, 48, 72h) tested (Prism, GraphPad Software, San Diego, CA). We used a one sample t-test to assess whether alignment (either parallel for $S>0$ or perpendicular for $S<0$) varied significantly from a hypothetical mean of $S=0$ (random alignment) at each of our experimentally tested frequencies. We did not run statistics on any of the measurements taken from Jungbauer (22).

Computational Model

As detailed in the SI Appendix, we modified a previously published model by Vigliotti et al. (15) and used it to simulate the experiments reported here. The model represents the thermodynamics of stress fiber assembly and disassembly and was previously shown to reproduce a number of experimentally observed cellular responses to a range of cyclic stretch waveforms applied to cells cultured on deformable 2D substrates. The model incorporates the fundamental observation that tension promotes stress fiber assembly by assuming that tension reduces the free energy of subunits in

the bound state. It also incorporates force-length and force-velocity behavior for actomyosin, allowing it to capture phenomena such as the disassembly of stress fibers in response to rapid shortening (15). The Vigliotti model was designed to simulate the response of a single cell to known applied strains. However, cells embedded in collagen gels can locally remodel both the collagen fibers and their attachments to the collagen (7, 24–26) over time scales of minutes to hours, so that the effective cell strain at any time point in our experiments likely differed from the gross compaction strains we measured using markers. We therefore introduced the additional assumption that over long time scales, the cell maintains an average stress state that minimizes its free energy. Furthermore, embedded cells and the surrounding gel are mechanically in series, so that in very soft gels the cells experience only a fraction of the applied cyclic strain (27). We therefore assumed that only a fraction of the applied cyclic strain was transmitted to cells when simulating 3D stretch, whereas the full applied cyclic strain was transmitted to cells when simulating 2D stretch.

Acknowledgments

This work was supported by NSF CMMI 1332530 (JWH) and NIH T32 GM008715 (KC). AV acknowledges support from the Royal Society's Newton International Fellowship Alumni Program.

References

1. Huang C, et al. (2013) Biological effects of cellular stretch on human dermal fibroblasts. *J Plast Reconstr Aesthetic Surg* 66(12):e351-61.

2. Moretti M, Prina-Mello A, Reid AJ, Barron V, Prendergast PJ (2004) Endothelial cell alignment on cyclically-stretched silicone surfaces. *J Mater Sci Mater Med* 15(10):1159–1164.

3. Kaunas R, Nguyen P, Usami S, Chien S (2005) Cooperative effects of Rho and mechanical stretch on stress fiber organization. *Proc Natl Acad Sci U S A* 102(44):15895–900.

4. Ives CL, Eskin SG, McIntire L V. (1986) Mechanical effects on endothelial cell morphology: In vitro assessment. *Vitr Cell Dev Biol* 22(9):500–507.

5. Karlon WJ, et al. (1999) Measurement of Orientation and Distribution of Cellular Alignment and Cytoskeletal Organization. *Ann Biomed Eng* 27(6):712–720.

6. Hsu HJ, Lee CF, Kaunas R (2009) A dynamic stochastic model of frequency-dependent stress fiber alignment induced by cyclic stretch. *PLoS One* 4(3):e48531-8.

7. Lee EJ, Holmes JW, Costa KD (2008) Remodeling of engineered tissue anisotropy in response to altered loading conditions. *Ann Biomed Eng* 36(8):1322–1334.

8. Foolen J, Deshpande VS, Kanters FMW, Baaijens FPT (2012) The influence of matrix integrity on stress-fiber remodeling in 3D. *Biomaterials* 33(30):7508–18.

9. Matsumoto T, et al. (2007) Three-Dimensional Cell and Tissue Patterning in a Strained Fibrin Gel System. *PLoS One* 2(11):e1211.

10. Roby T, Olsen S, Nagatomi J (2008) Effect of Sustained Tension on Bladder Smooth Muscle Cells in Three-Dimensional Culture. *Ann Biomed Eng* 36(10):1744–1751.

11. Bellows CG, Melcher AH, Aubin JE (1982) Association between tension and orientation of periodontal ligament fibroblasts and exogenous collagen fibres in collagen gels in vitro. *J Cell Sci* 58(1):125–38.

12. Hu J-J, Humphrey JD, Yeh AT (2009) Characterization of engineered tissue development under biaxial stretch using nonlinear optical microscopy. *Tissue Eng Part A* 15(7):1553–1564.

13. Pang Y, Wang X, Lee D, Greisler HP (2011) Dynamic quantitative visualization of single cell alignment and migration and matrix remodeling in 3-D collagen hydrogels under mechanical force. *Biomaterials* 32(15):3776–83.

14. Obbink-Huizer C, et al. (2014) Computational model predicts cell orientation in response to a range of mechanical stimuli. *Biomech Model Mechanobiol* 13(1):227–36.

15. Vigliotti A, Ronan W, Baaijens FPT, Deshpande VS (2016) A thermodynamically motivated model for stress-fiber reorganization. *Biomech Model Mechanobiol* 15(4):761–789.

16. Costa KD, Lee EJ, Holmes JW (2003) Creating Alignment and Anisotropy in Engineered Heart Tissue: Role of Boundary Conditions in a Model Three-Dimensional Culture System. *Tissue Eng* 9(4):567–577.

17. Thomopoulos S, Fomovsky GM, Chandran PL, Holmes JW (2007) Collagen fiber alignment does not explain mechanical anisotropy in fibroblast populated collagen gels. *J Biomech Eng* 129(5):642–50.

18. Knezevic V, Sim a J, Borg TK, Holmes JW (2002) Isotonic biaxial loading of fibroblast-populated collagen gels: a versatile, low-cost system for the study of mechanobiology. *Biomech Model Mechanobiol* 1(1):59–67.

19. De Jonge N, Kanters FMW, Baaijens FPT, Bouten CVC (2013) Strain-induced collagen organization at the micro-level in fibrin-based engineered tissue constructs. *Ann Biomed Eng* 41(4):763–774.

20. Terracio L, Miller B, Borg TK (1988) Effects of cyclic mechanical stimulation of the cellular components of the heart: In vitro. *Vitr Cell Dev Biol* 24(1):53–58.

21. Hsu H-J, Lee C-F, Locke A, Vanderzyl SQ, Kaunas R (2010) Stretch-Induced Stress Fiber Remodeling and the Activations of JNK and ERK Depend on Mechanical Strain Rate, but Not FAK. *PLoS One* 5(8):e12470.

22. Jungbauer S, Gao H, Spatz JP, Kemkemer R (2008) Two Characteristic Regimes in Frequency-Dependent Dynamic Reorientation of Fibroblasts on Cyclically Stretched Substrates. *Biophys J* 95(7):3470–3478.

23. Deshpande VS, McMeeking RM, Evans AG (2006) A bio-chemo-mechanical model for cell contractility. *Proc Natl Acad Sci U S A* 103(38):14015–20.

24. Moon AG, Tranquillo RT (1993) Fibroblast-populated collagen microsphere assay of cell traction force: Part 1. Continuum model. *AIChE J* 39(1):163–177.

25. Pizzo AM, Kokini K, Vaughn LC, Waisner BZ, Voytik-Harbin SL (2005) Extracellular matrix (ECM) microstructural composition regulates local cell-ECM biomechanics and fundamental fibroblast behavior: a multidimensional perspective. *J Appl Physiol* 98(5):1909–21.

26. Kim A, Lakshman N, Petroll WM (2006) Quantitative assessment of local collagen matrix remodeling in 3-D Culture: The role of Rho kinase. *Exp Cell Res*

312(18):3683–3692.

27. Ujihara Y, et al. (2015) Computational studies on strain transmission from a collagen gel construct to a cell and its internal cytoskeletal filaments. *Comput Biol Med* 56:20–29.

28. Kaunas R, Hsu HJ (2009) A kinematic model of stretch-induced stress fiber turnover and reorientation. *J Theor Biol* 257(2):320–330.

29. De R, Zemel A, Safran S a. (2007) Dynamics of cell orientation. *Nat Phys* 3(9):655–659.

30. Rouillard AD, Holmes JW (2014) Mechanical Boundary Conditions Bias Fibroblast Invasion in a Collagen-Fibrin Wound Model. *Biophys J* 106(4):932–943.

31. Batschelet E (1981) *Circular Statistics in Biology* (Academic Press, London, London).

Figure Legends

Figure 1: Experimental Setup and Test Conditions. **A)** Fibroblast-populated collagen gels with sponges embedded in the arms. During an initial pre-culture period, gel arms would either be biaxially constrained with pins (circled) or left to float freely in media and isotropically compact. Square box indicates region of interest painted with 9 TiO_2 dots to track gel deformations and later imaged to assess cell alignment. **B)** Collagen gel (cruciform shaped box) pinned in CellScale device. Scale bars=1cm. **C,D)** Collagen gels initially cultured under biaxial constraint before being subjected to **C)** 0 or 10% uniaxial stretch in the x_1 direction (x_2 left free) or **D)** 0 or 10% strip uniaxial stretch in x_1 (x_2 held fixed). **E)** Collagen gels initially allowed to compact isotropically before being subjected to either 0 or 10% uniaxial stretch in x_1. All conditions tested for 24, 48, and 72h. Diagonal lines indicate constraint; arrows indicate direction of cyclic stretch; dashed boxes indicate original gel size before compaction.

Figure 2: Time course of gel deformation and cell alignment at 24, 48, and 72h. After an initial pre-culture period (**black x**), collagen gels were subjected to either 0% stretch (**open symbols**) or 10% (0.5 Hz) stretch (**closed symbols**). Compaction deformations in the x_1 (F_{11}: **A,D,G**) and x_2 (F_{22}: **B,E,H**) directions were measured using titanium oxide markers. Average mean vector length (MVL^{gel}: **C,F,I**) describes the strength of cell alignment. Mean angle of all uniaxial cases was 0^o. (*******ANOVA $p<0.001$ difference over time, $^{+++}$ANOVA $p<0.001$ difference between 0% and 10% groups). Each data point is representative of five independent experiments and expressed as the mean $\pm$ SD.

Figure 3: In all uniaxial cases, cells aligned with similar strength in the direction of stretch, regardless of the pattern of compaction (anisotropic vs. isotropic) or the presence of cyclic stretch. Angular histograms of cell orientation for 0% stretch (**open symbols**, row 1: **A,D,G**) or 10% (0.5 Hz) stretch (**closed symbols**, row 2: **B,E,H**) at 72 hour time points. Each data point is representative of five independent experiments and expressed as the mean ± SD. Angular histograms of stress fiber orientation from computational simulations of our test conditions (row 3: **C,F,I**). In agreement with the experimental findings, the model predicted uniformly distributed stress fibers along the x_1 axis under uniaxial stretch (**C,F**) and uniformly distributed SFs under strip uniaxial stretch (**I**). Dotted lines indicate 0% stretch and solid lines indicate 10% cyclic (0.5 Hz) stretch. *Insets* show circular histogram representations of stress fibers for 0% cases.

Figure 4: The model captures alignment trends across a range of frequencies and boundary conditions in both 3D and 2D culture conditions. We plotted the order parameter $S=\langle\cos 2\theta\rangle$ that quantifies alignment (1 = parallel, -1 = perpendicular, 0 = random) as a function of frequency in 3D uniaxial cyclic stretch (**blue triangles**), 3D strip uniaxial cyclic stretch (**green squares**), and 2D cyclic stretch on silicone elastomer membranes (**grey diamonds**) in experimentally measured cell orientations (**A**) and computationally predicted stress fiber orientations (**B**). Each data point for the experimental conditions is expressed as the mean ± SD. 3D data points represent five independent experiments (except uniaxial 4 Hz, n=4) (***$p<0.001$, *$p<0.05$), while 2D data points represent 30-50 cells measured by Jungbauer et al. (22) in rat embryonic fibroblasts at 8% cyclic stretch.

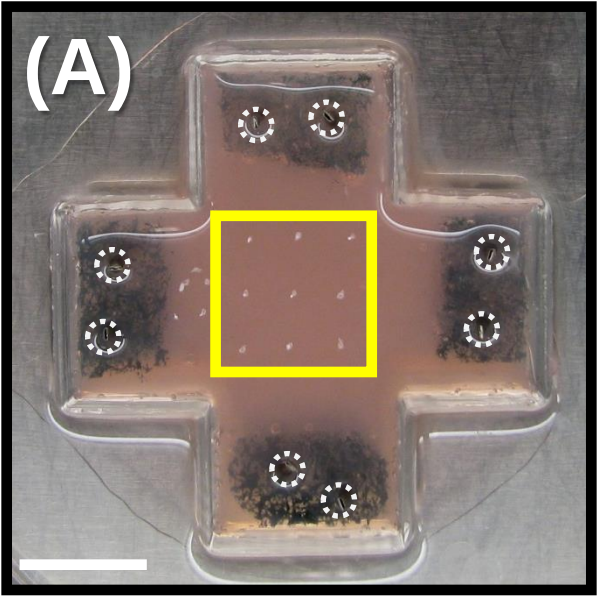

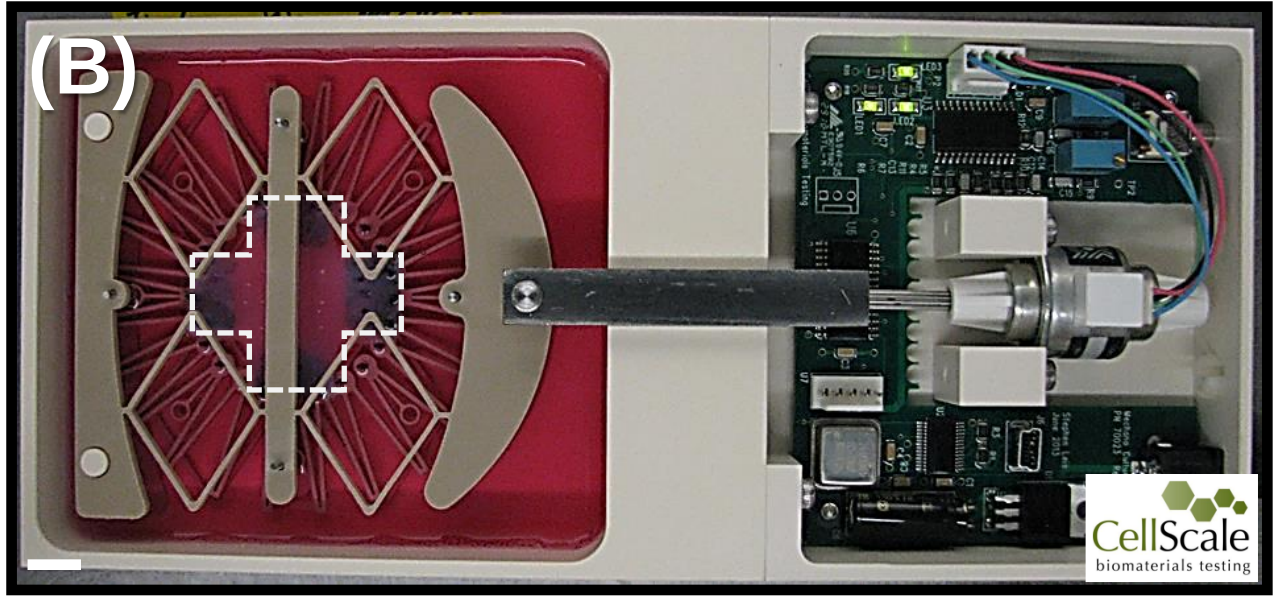

Pre-culture:

Biaxial Constraint

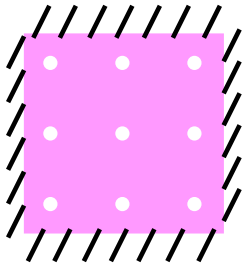

Free to Compact

Stretch (Cyclic):

(C) 0 & 10% Uniaxial

(D) 0 & 10% Strip Uniaxial

(E) 0 & 10% Uniaxial

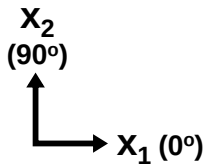

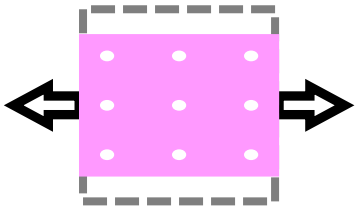

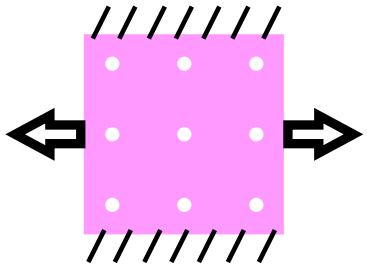

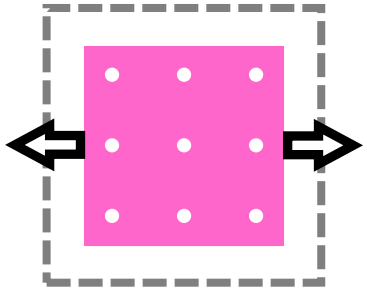

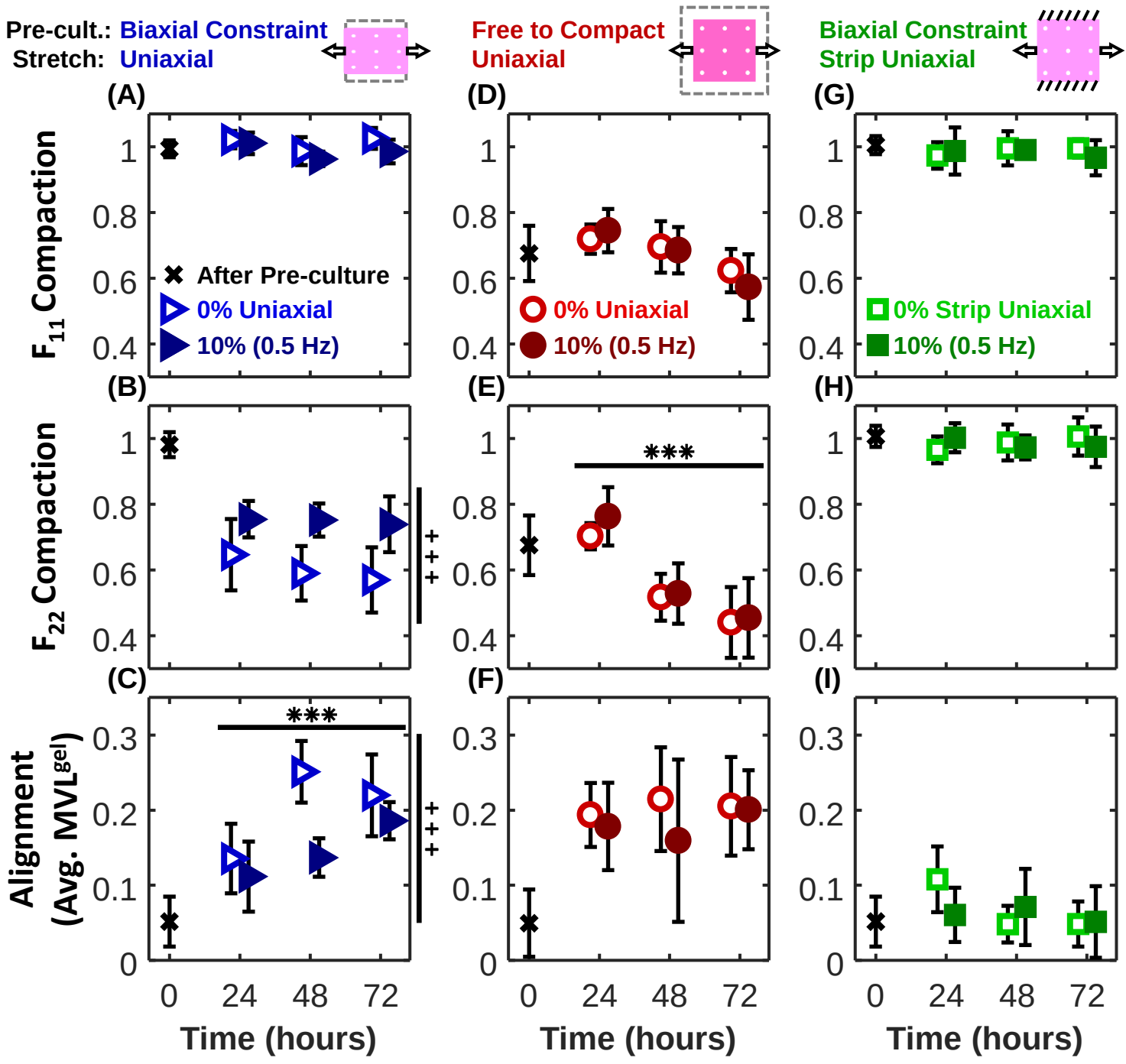
Pre-cult.: Biaxial Constraint
Stretch: Uniaxial
Free to Compact Uniaxial
Biaxial Constraint Strip Uniaxial
(A)
(B)
(C)
(D)
(E)
(F)
(G)
(H)
(I)
F11 Compaction
F22 Compaction
Alignment (Avg. MVL^gel)
After Pre-culture
0% Uniaxial
10% (0.5 Hz)
0% Strip Uniaxial
***
+++
Time (hours)
0
24
48
72
0.4
0.6
0.8
1
0
0.1
0.2
0.3

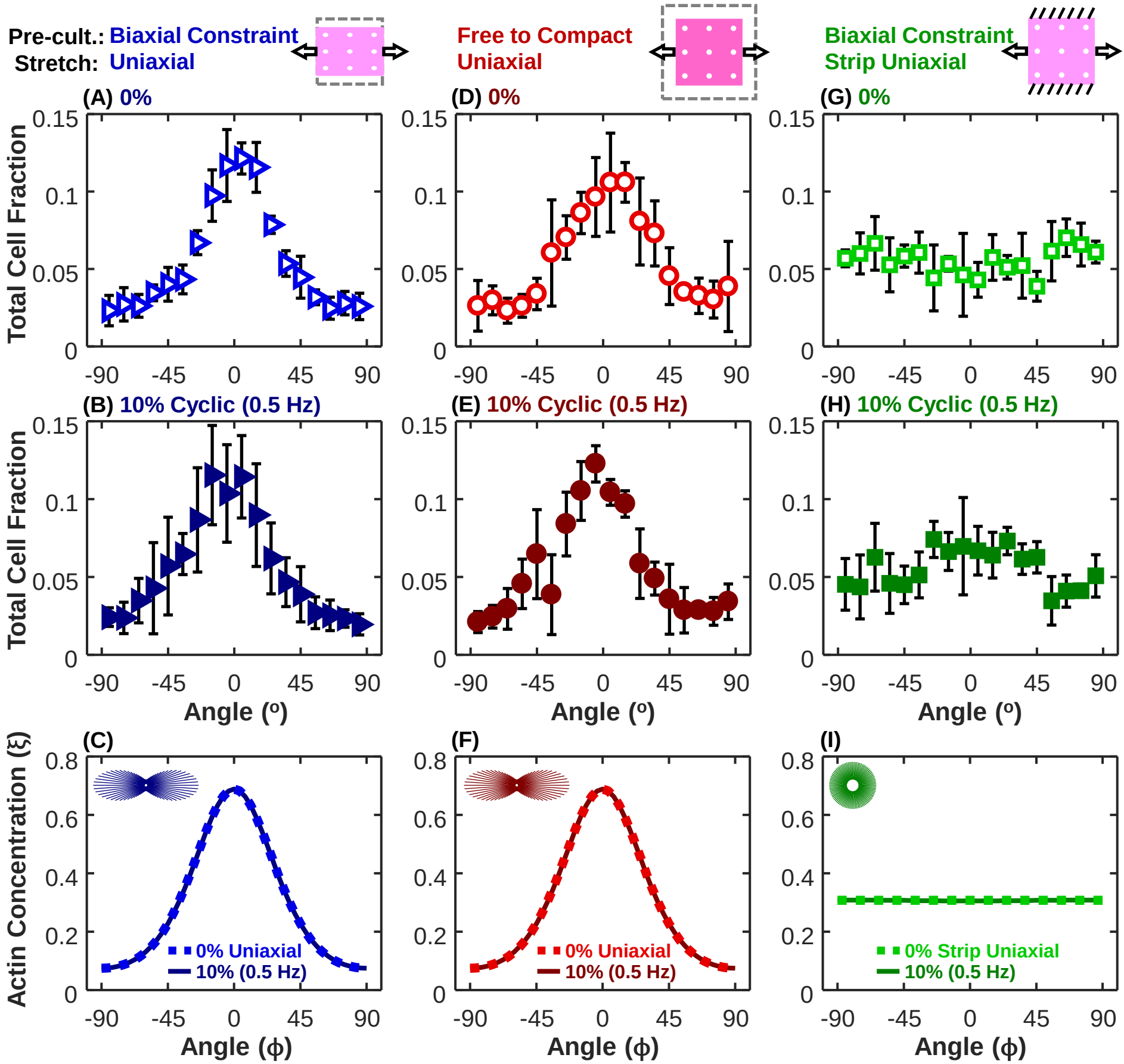
Pre-cult.: Biaxial Constraint
Stretch: Uniaxial
Free to Compact Uniaxial
Biaxial Constraint Strip Uniaxial
(A) 0%
(D) 0%
(G) 0%
(B) 10% Cyclic (0.5 Hz)
(E) 10% Cyclic (0.5 Hz)
(H) 10% Cyclic (0.5 Hz)
Total Cell Fraction
Angle (º)
(C)
(F)
(I)
Actin Concentration (ξ)
0% Uniaxial
10% (0.5 Hz)
0% Strip Uniaxial
Angle (ϕ)

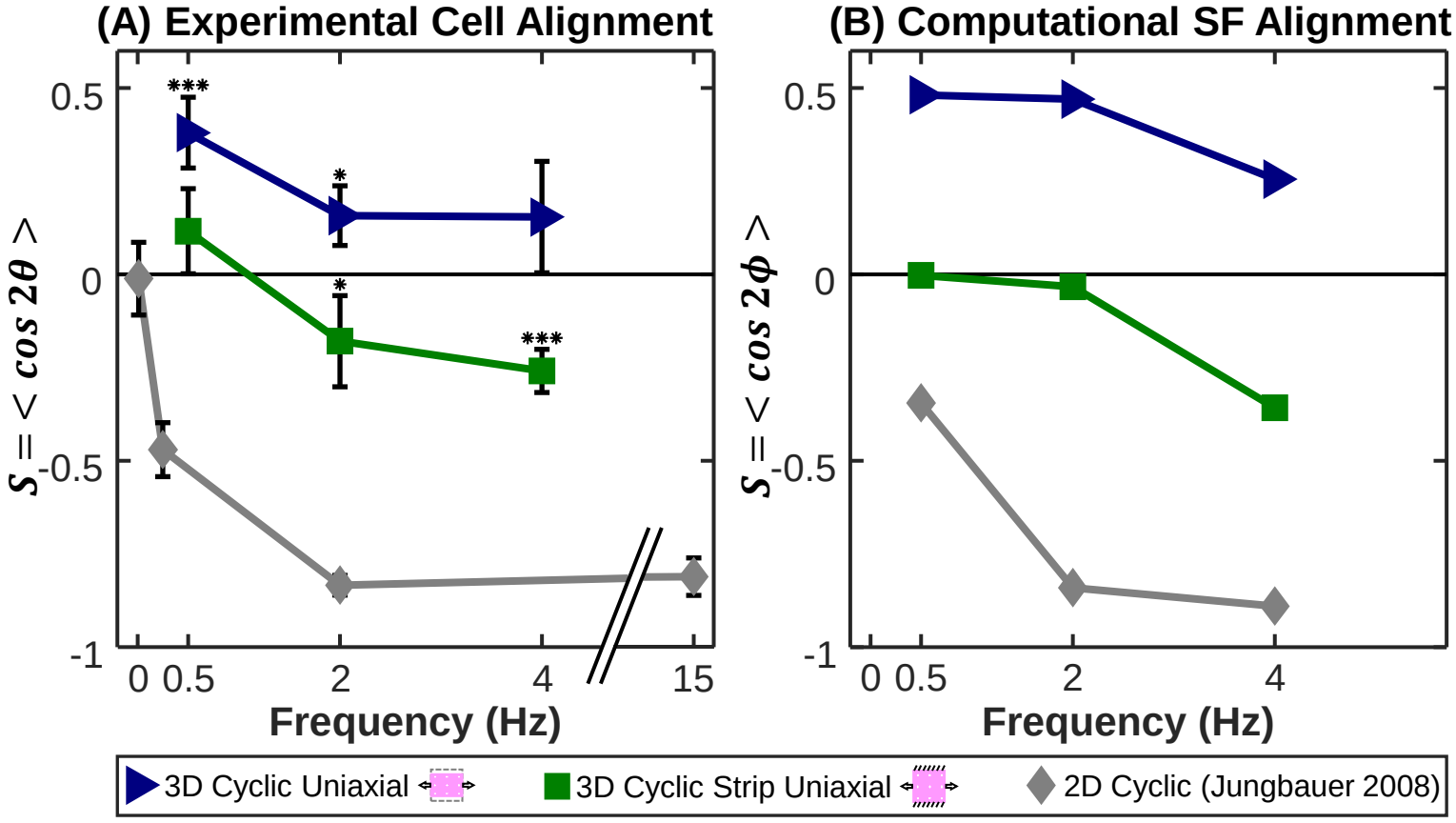
(A) Experimental Cell Alignment
(B) Computational SF Alignment
0.5
0
-0.5
-1
$S = \langle \cos 2\theta \rangle$
$S = \langle \cos 2\phi \rangle$
***
*
*
***
0
0.5
2
4
15
Frequency (Hz)
3D Cyclic Uniaxial
3D Cyclic Strip Uniaxial
2D Cyclic (Jungbauer 2008)

Supporting Information

Adult Cardiac Fibroblast Isolation and Culture

We euthanized Sprague-Dawley rats (6 weeks old, ~220 g), removed and minced their ventricles into ~1 mm^3 pieces, and digested the pieces using Liberase TM Research Grade (Roche, Indianapolis, IN). We centrifuged successive digestions for 10 min at 400 x *g,* resuspended the cells in culture medium containing Dulbecco's modified Eagle medium (Sigma-Aldrich, St. Louis, MO) with 10% fetal bovine serum (FBS, Atlanta Biologicals, Flowery Branch, GA), 100 U/mL penicillin, 100 μg/mL streptomycin, and 2 ng/mL amphotericin B (all Sigma-Aldrich), and transferred the cells into cell culture flasks incubated at 37°C and 5% CO_2. After 4h, we removed the culture media, rinsed the cells with phosphate-buffered saline (PBS, Sigma-Aldrich) to remove nonadherent cells, and resupplied with culture medium. We replaced media every 2-3 days and harvested cells for experiments at passage 1 (7 days after isolation) or 2 (10-11 days after isolation).

Fabrication of Fibroblast-Populated Collagen Hydrogels

We serum starved the fibroblasts for 18 hours before using 0.25% Trypsin-EDTA (Sigma-Aldrich) to dissociate them from their flasks and resuspending them in serum-free culture media. We created collagen solution at a 1:1:8 ratio of 0.2 M HEPES, 10X MEM (both Sigma-Aldrich), and 3.1 mg/mL type I Bovine Collagen Solution (PureCol, Advanced Biomatrix, San Diego, CA) and mixed it at a 4:1 ratio with the resuspended cells for a final cell concentration of 200k cells/mL and collagen concentration of ~2mg/mL. We placed this cell+collagen mixture on a rotator in an incubator for 20-30 min to initiate gelation before pouring it into 100mm x 15mm Petri dishes coated with polydimethylsiloxane (PDMS, Dow Corning,

Sylgard 184 Silicone Elastomer Kit) to prevent adhesion and fitted with negative cruciform molds with small sponges at the arms (Fig. 1A). After the gels polymerized for 4h in an incubator, we either isotropically constrained them for 1 day by pushing two small pins through each sponge into the PDMS layer, or we let them float freely in media and isotropically compact for 1 day. The free-floating gels were cast from a larger total volume in larger molds to allow for compaction, so that dimensions of all gels would be matched after 1 day, prior to transfer to the loading system.

Comparison of Cell Alignment to Stress Fiber Alignment

Our experiments quantified the orientation distribution of populations of cells, while most models (including the one employed here, see below) predict distributions of stress fibers (SFs) within a single hypothetical cell. In order to understand any differences between these two metrics that might confound interpretation, we imaged ten cells from each 72h loading condition (sixty total) with a confocal microscope with a 60x objective, creating z-stacks consisting of one image every 0.5μm through each cell's thickness. Within each z-stack, we created 2D grayscale projections by manually selecting images that most clearly showed the cell's SFs. We measured stress fiber orientation using the custom software MatFiber, a MATLAB implementation of an intensity-gradient-detection algorithm originally developed by Karlon et al. (1) and subsequently used by our group to quantify collagen fiber orientation in histologic sections (2, 3) and by others to quantify stress fiber alignment within stretched cells (4, 5). We used the orientations of structures within 6x6 pixel subregions to calculate the strength of alignment, MVL^{SF} (ranging from 0, all SFs randomly oriented, to 1, all SFs aligned) and mean angle, MA^{SF} (see main

manuscript, equations 2-4). Then, the boundaries of each cell were traced to calculate each cell's MA^{cell} and MVL^{cell} as described above for comparison.

The calculated orientation of the cell using its boundary, MA^{cell}, and its stress fibers, MA^{SF}, correlated closely across most of the 60 cells analyzed, with an overall regression equation $MA^{cell} = 0.88*MA^{SF} - 7.2$ and an R^2 value of 0.84 (Fig. S1A). The strength of orientation of the cell using its boundary, MVL^{cell}, and its stress fibers, MVL^{SF} were less tightly correlated on a cell-by-cell basis, with an R^2 value of 0.65 (Fig. S1B); the relationship between these two measures ($MVL^{cell} = 1.25*MVL^{SF} + 0.08$) suggested that mean vector length computed from the cell boundary is generally higher than the mean vector length computed from stress fibers imaged in the same cell.

Modified Computational Model

Here we describe briefly describe the model of Vigliotti et al. (6) and its application for the analysis of cells in tissues subjected to different boundary conditions as described in the main manuscript. We restrict attention to a 2D cell in the $x_1 - x_2$ plane with the out-of-plane Cauchy stress $\Sigma_{33} = 0$.

Configuration Under Static Loading

The Vigliotti et al. (6) model describes the kinetics of stress-fiber remodeling for a given set of boundary conditions. The internal chemical kinetic processes (formation/dissociation of stress-fibers and diffusion of the unbound stress-fiber proteins) are rapid and attain an equilibrium rapidly compared to the rate at which the cell can change its morphological configuration (i.e. its shape, size etc). Thus, under static loading conditions the observed state is well approximated by the equilibrium state of the cell. In order to determine that equilibrium state for a given

set of boundary conditions, we use the Vigliotti model to calculate the Gibbs-free energy of the cell as outlined below.

Let b_0 be the thickness of the 2D cell in its elastic resting state and the corresponding volume V_0. The reference representative volume element (RVE) of the stress-fibers within the cell in this resting configuration is assumed to be a cylinder of volume $V_R = \pi b_0 \left(\frac{n^R \ell_0}{2}\right)^2$ where ℓ_0 is the length of a stress-fiber functional unit in its ground-state and n^R the number of these ground-state functional units within the undeformed circular cell. The total number of functional unit packets within the cell is N_0^T and we introduce $N_0 = N_0^T V_R / V_0$ as the average number of functional unit packets available per RVE; N_0 shall serve as a useful normalisation parameter. The state of the stress-fibers at location x_i within the cell is described by their angular concentration $\eta(\phi, x_i)$, and the number $n(\phi, x_i)$ of the functional units in series along the length of each stress-fiber in the RVE, where ϕ is the angle with respect to the x_1 direction. Vigliotti et al. (6) argue that an applied stretch is shared equally among all subunits, so that the strain within each functional unit $\tilde{\varepsilon}_n$, is initially equal to the nominal strain $\varepsilon_n(x_i, \phi)$ in direction ϕ. Subsequent addition or removal of subunits modifies the subunit stretch proportionally so that, at steady-state, the number n^{ss} of functional units within the stress fibers is given by

$$\hat{n}^{ss} \equiv \frac{n^{ss}}{n^R} = \frac{[1 + \varepsilon_n(x_i, \phi)]}{1 + \tilde{\varepsilon}_n^{ss}}, \tag{A1}$$

where $\tilde{\varepsilon}_n^{ss}$ is the strain at steady-state within a functional unit of the stress fibers. In order to calculate the steady-state angular concentration of the stress fibers, we

begin with the chemical potential of the functional units within the stress fibers as derived by Vigliotti et al. (6) as

$$\chi_b = \frac{\mu_b^{ss}}{n^R} + kT\ln\left[\left(\frac{\pi\hat{\eta}\,\hat{n}^{ss}}{\widehat{N}_u}\right)^{\frac{1}{n^{ss}}}\left(\frac{\widehat{N}_u}{\pi\widehat{N}_L}\right)\right], \tag{A2}$$

where $\widehat{N}_u$ is the normalized concentration of the unbound stress fiber proteins given by $\widehat{N}_u \equiv N_u/N_0$ and $\hat{\eta} \equiv \eta n^R/N_0$ is the normalized angular density of stress-fibers. Here $\widehat{N}_L$ is the number of available lattice sites while the enthalpy of n^R bound functional units at steady-state is given in terms of the isometric stress-fiber stress $\sigma_{\max}$ and the internal energy μ_{b0} as

$$\mu_b^{ss} = \mu_{b0}[1 + \beta(\tilde{\varepsilon}_n^{ss})^2] - \sigma_{\max}(1 + \tilde{\varepsilon}_n^{ss})\Omega, \tag{A3}$$

where Ω is the volume of n^R functional units. The chemical potential of the unbound proteins in terms of the internal energy μ_u is

$$\chi_u = \frac{\mu_u}{n^R} + kT\,\ln\left(\frac{\widehat{N}_u}{\pi\,\widehat{N}_L}\right). \tag{A4}$$

Equating the chemical potentials (A2) and (A4) and denoting the steady-state values of $\widehat{N}_u$ and $\hat{\eta}$ by $\widehat{N}_u^{ss}$ and $\hat{\eta}^{ss}$, respectively, provides the following relation between these quantities:

$$\hat{\eta}^{ss}(x_i,\phi) = \frac{\widehat{N}_u^{ss}}{\pi\,\hat{n}^{ss}(x_i,\phi)}\exp\left[\hat{n}^{ss}\frac{\mu_u - \mu_b^{ss}(x_i,\phi)}{kT}\right]. \tag{A5}$$

We emphasize that $\widehat{N}_u^{ss}$ is a constant, i.e. independent of x_i as the chemical potential (A4) at equilibrium is constant over the entire cell. We can now use conservation of

the stress-fiber proteins to determine $\widehat{N}_u^{ss}$. The normalized total number of functional unit packets $\widehat{N}_T \equiv N_T/N_0$ in a RVE located at x_i follows from the above analysis as

$$\widehat{N}_T(x_i) = \widehat{N}_u^{ss}(x_i)\left[1 + \frac{1}{\pi}\int_{-\frac{\pi}{2}}^{\frac{\pi}{2}} \exp\left[\hat{n}^{ss}\frac{\mu_u - \mu_b^{ss}(x_i,\phi)}{kT}\right]d\phi\right], \tag{A6}$$

with conservation of the proteins then specifying

$$\frac{1}{A_0}\int_{A_0} \widehat{N}_T\, dA = 1, \tag{A7}$$

where $A_0 \equiv V_0/b_0$ is the resting area of the cell. Combining (A6) and (A7),

$$\widehat{N}_u^{ss} = \frac{1}{1 + \frac{1}{A_0\pi}\int_{A_0}\int_{-\frac{\pi}{2}}^{\frac{\pi}{2}} \exp\left[\hat{n}^{ss}\frac{\mu_u - \mu_b^{ss}(x_i,\phi)}{kT}\right]d\phi\, dA}. \tag{A8}$$

The cytoskeletal free-energy is then

$$G_{cyto} = \frac{N_0 b_0}{V_R}\int_{A_0}\left[\widehat{N}_u^{ss}\chi_u^{ss} + \int_{-\frac{\pi}{2}}^{\frac{\pi}{2}} \hat{\eta}\hat{n}\chi_b^{ss}d\phi\right]dA = \chi_u^{ss}N_0^T, \tag{A9}$$

where χ_u^{ss} and χ_b^{ss} are the steady-state values of χ_u and χ_b, respectively.

To complete the description of the cell we need to specify the stress state. Vigliotti et al. (6) showed via a homogenization analysis that in 2D the stress state due to the active stresses generated by the stress-fibers is given by

$$\begin{bmatrix}\sigma_{11} & \sigma_{12}\\ \sigma_{12} & \sigma_{22}\end{bmatrix} = f_0\sigma_{\max}\int_{-\pi/2}^{\pi/2} \hat{\eta}^{ss}[1+\varepsilon_n(\phi)]\begin{bmatrix}\cos^2\phi^* & \frac{\sin 2\phi^*}{2}\\ \frac{\sin 2\phi^*}{2} & \sin^2\phi^*\end{bmatrix}d\phi, \tag{A10}$$

where ϕ^* is the angle of the stress-fiber measured with respect to x_i and is related to ϕ by the rotation of the base vectors e_i from the reference configuration and f_0 is the

volume fraction of stress-fiber proteins under reference conditions. The total Cauchy stress Σ_{ij} follows from an additive decomposition of σ_{ij} and the passive stress σ_{ij}^{p} as

$$\Sigma_{ij} = \sigma_{ij} + \sigma_{ij}^{p}. \tag{A11}$$

The passive response is assumed to follow a compressible Neo-Hookean relation of the form

$$W = \frac{E}{4(1+\nu)}\left[J^{-2/3}\sum_{j=1}^{3}\lambda_j^2 - 3\right] + \frac{E}{6(1-2\nu)}[J-1]^2, \tag{A12}$$

where E and ν are the Young's modulus and Poisson's ratio, respectively, λ_j are the three principal stretches and $J \equiv \lambda_1\lambda_2\lambda_3$. The principal components of the passive Cauchy stress are given as

$$\sigma_i^{p} \equiv \frac{\lambda_i}{J}\frac{\partial W}{\partial \lambda_i}. \tag{A13}$$

The specification is complete by requiring mechanical equilibrium, i.e.

$$\frac{\partial \Sigma_{ij}}{\partial x_j} = 0, \tag{A14}$$

subject to the appropriate boundary conditions. The total free-energy of the cell is then

$$G = G_{cyto} + b_0 \int_{A_0} W dA, \tag{A15}$$

which reduces to the expression

$$g \equiv g_{cyto} + g_{elas} = \rho_0 \chi_u^{ss} + \frac{1}{A_0}\int_{A_0} W dA, \tag{A16}$$

for the free-energy of the cell per unit volume. Here, $\rho_0 \equiv N_0^T/V_0$ is the volumetric concentration of the stress-fiber proteins with $g_{cyto} \equiv \rho_0 \chi_u^{ss}$ the cytoskeletal free-energy per unit volume and g_{elas} the corresponding elastic energy per unit volume.

Now consider the case of a low density of fibroblasts seeded in the gels or on 2D flat substrates such that the cells do not directly interact with each other. The cells adhere to the collagen or other fibers in the gel or ligands on the substrate and remodel their shape and size so as to minimize their free-energy. In the 2D context being analyzed here we model the cells lying in the $x_1 - x_2$ plane with $\Sigma_{33} = 0$. The gel is a weak plastically deforming medium and thus can only sustain stresses exerted by the cell that are balanced by the applied boundary conditions. Furthermore, the local plastic deformation of the gel near each individual cell is unknown. We simplify the problem by modeling the cells to be spatially uniform, described by a single set of nominal strains E_{11}, E_{22} and E_{12}. The above analysis to calculate the free-energy of the cell then simplifies considerably with

$$\widehat{N}_u^{ss} = \frac{1}{1 + \frac{1}{\pi}\int_{-\frac{\pi}{2}}^{\frac{\pi}{2}} \exp\left[\hat{n}^{ss}\frac{\mu_u - \mu_b^{ss}(x_i,\phi)}{kT}\right] d\phi}, \tag{A17}$$

and

$$g = \rho_0\left[\frac{\mu_u}{n^R} + kT\ln\left(\frac{\widehat{N}_u^{ss}}{\pi\,\widehat{N}_L}\right)\right] + g_{elas}, \tag{A18}$$

where in this simplified setting $g_{elas} = W$. The simulations were performed with the following set of parameters taken from Vigliotti et al. (6). All simulations are reported for cells at a temperature $T = 310$ K. The passive elastic parameters are taken to be $E = 5.0$ kPa and ν =0.45, while the maximum contractile stress $\sigma_{\max} = 240$ kPa and volume fraction $f_0 = 0.032$. The internal energies of the unbound and bound proteins are $\mu_u = 8\, k_B T_0$ and $\mu_{b0} = 9\, k_B T_0$, where $T_0 = 310$ K with $\beta = 1.2$ while the reference volume of n^R functional units is taken to be $\Omega = 10^{-7.1}\,\mu\text{m}^3$. The volumetric concentration ρ_0 of the proteins was not specified in Vigliotti et al. (6) as the free-energy was not explicitly calculated. All simulations reported here use $\rho_0 = 1.5 \times 10^5 \mu\text{m}^{-3}$.

We now proceed to detail the analysis for the three cases under consideration here: (i) biaxial constraint imposed on the gel; (ii) gels restrained uniaxially in the x_1 direction; and (iii) cells on stiff and flat 2D substrates. For the case of biaxial restraint, the applied boundary conditions can balance any stresses Σ_{11} and Σ_{22} generated by the cell but the gel cannot sustain a shear stress Σ_{12} generated by the cell. Thus, we constrain the cells to only assume states with $E_{12} = 0$ so that no elastic shear stresses are generated. Moreover, the boundary conditions in the x_1 and x_2 directions are identical and thus it is reasonable to assume that cells assume states with $E_{11} = E_{22}$. The cells then spread and remodel within the gel subject to these constraints in order to minimize their free-energy g. We define a normalised cytoskeletal and total free-energies as

$$\hat{g}_{cyto} = \frac{g_{cyto} - \rho_0 \mu_u / n^R + kT \ln(\pi \hat{N}_L)}{\rho_0 \mu_u} = \frac{kT}{\mu_u} \ln\left(\hat{N}_u^{ss}\right), \tag{A19}$$

and

$$\hat{g} = \frac{g - \rho_0\mu_u/n^R + kT\ln(\pi\widehat{N}_L)}{\rho_0\mu_u} = \frac{kT}{\mu_u}\ln\left(\widehat{N}_u^{ss}\right) + \hat{g}_{elas}, \qquad \text{(A20)}$$

respectively where $\hat{g}_{elas} \equiv W/(\rho_0\mu_u)$. Here we have subtracted $[\rho_0\mu_u/n^R - kT\ln(\pi\widehat{N}_L)]$ in defining the normalized energies as this term is a constant that does not vary with the state of the cell. A minimum is seen at $E_{11}^{opt} = E_{22}^{opt} = 0.062$; this represents the state that the cell assumes under static loading with this boundary condition (Fig. S1A), and the predicted distribution of assembled actin $\xi^{ss} \equiv \hat{\eta}^{ss}(\phi)\hat{n}^{ss}(\phi)$ is spatially isotropic (Fig. 3I). The configuration of cells under static loading on 2D flat substrates is identical to that for the biaxially constrained gel as the 2D stiff substrates can support any stresses/tractions generated by the cell in the x_1 and x_2 directions.

For the case of uniaxial restraint in the x_1 direction, equilibrium requires that resultant forces in the x_2 direction vanish, so we only allow the cells to assume states with $\Sigma_{22} = 0$. As in the biaxial case, we also assume the gel cannot support shear stresses Σ_{12} so that $E_{12} = 0$. Thus, the problem reduces to determining the value of E_{11} that minimizes $\hat{g}$. A minimum is seen at $E_{11}^{opt} = 0.075$, $E_{22}^{opt} = -0.2107$ (Fig. S1B,C) and is associated with preferential alignment of stress fibers along the x_1 direction (Fig. 3C,F).

Analysis of Fibroblast-Populated Gels Under Cyclic Loading

To simulate cyclic loading of cells (on 2D substrates and in gels) we separate the strain E_{ij} of the cell into two parts: a static time independent component $\bar{E}_{ij}$ and a cyclic component $\Delta E_{ij}(t)$ such that $E_{ij}(t) = \bar{E}_{ij} + \Delta E_{ij}(t)$. We assume that over long time scales the cells can remodel such that they adjust their connection to the gel or

the substrate and adjust $\bar{E}_{ij}$ so as to minimize their free-energy subject to the appropriate boundary conditions. Thus, the calculation of $\bar{E}_{ij}$ reduces to the free-energy minimization of the cell under equivalent static boundary conditions as outlined above. It now remains to specify the response of cells subject to the additional time-dependent strains $\Delta E_{ij}(t)$.

The cyclic analysis of the cells in the gels differed from that for cells on the 2D substrates. Cells on 2D substrates are adhered to the substrates and the cyclic strains $\Delta e_{ij}(t)$ applied to the substrate are directly transmitted to the cell, i.e. $\Delta E_{ij}(t) = \Delta e_{ij}(t)$. However, for cells within very soft 3D gels, the majority of the imposed strains are accommodated within the gel with only a small fraction δ transmitted to the cells (7), i.e. $\Delta E_{ij}(t) = \delta\, \Delta e_{ij}(t)$, where $0 \leq \delta \leq 1$.

We analyze the three cyclic loading cases using the full Vigliotti et al. (6) model, i.e. the model accounting for transient evolution of the cytoskeleton and not just the steady-state limit as described above. The three cyclic loading cases and the associated boundary conditions are:

(i) Cyclic response of cells on 2D substrates: here we impose $\Delta E_{11}(t) = \Delta e_{11}(t)$ with $\Delta E_{22}(t) = 0$.

(ii) Strip uniaxial stretch of cells in gels: here we impose $\Delta E_{11}(t) = \delta \Delta e_{11}(t)$ with $\Delta E_{22}(t) = 0$.

(iii) Uniaxial stretch of cells in gels: here we impose $\Delta E_{11}(t) = \delta \Delta e_{11}(t)$ with $\Sigma_{22}(t) = 0$.

The transient model of Vigliotti et al. (6) requires a few additional parameters to those specified above. These are taken from (6) but we list them here for the sake of completeness. The activation barrier for stress fiber kinetics is taken to be $\mu_a =$

$20\ k_B T_0$ while the time constant for stress fiber formation/dissociation is $\omega_n = 20\ \mathrm{Hz}$ with the stress-fiber remodeling assumed to be slow with a rate constant $\alpha = 0.01\ \mathrm{Hz}$. In addition we now need to specify the parameters for the dependence of the stress generated by the stress-fibers on the stress-fiber strain rates, which is assumed to have a Hill-like form with associated constants $\dot{\varepsilon}_0 = 0.53\ \mathrm{s}^{-1}$, $\varepsilon_p = 0.6$ and $\varepsilon_s = 0.3$. The cyclic simulations were performed with initial conditions given by the corresponding static analysis described above. Finally, the parameter δ that sets the cyclic strain transmitted into the cells in the gels was set to $\delta = 0.0125$ in all simulations reported here. Cyclic loading was imposed until a steady-state was attained which was realized for all boundary conditions after approximately 12 hours of cyclic loading. The cyclic steady-state distributions of $\xi \equiv \eta n$ as a function of ϕ are presented in Fig. 3C,F,I.

Supporting References

1. Karlon WJ, Covell JW, Mcculloch AD, Hunter JJ, Omens JH (1998) Automated measurement of myofiber disarray in transgenic mice with ventricular expression ofras. *Anat Rec* 252(4):612–625.

2. Fomovsky GM, Holmes JW (2010) Evolution of scar structure, mechanics, and ventricular function after myocardial infarction in the rat. *Am J Physiol Heart Circ Physiol* 298(1):H221-8.

3. Holmes JW (2015) Cardiac Biomechanics Group Downloads and Protocols. *Univ Virginia Acad Web Pages*. Available at: http://bme.virginia.edu/holmes/downloads/index.html.

4. Kaunas R, Nguyen P, Usami S, Chien S (2005) Cooperative effects of Rho and mechanical stretch on stress fiber organization. *Proc Natl Acad Sci U S A* 102(44):15895–900.

5. Karlon WJ, et al. (1999) Measurement of Orientation and Distribution of Cellular Alignment and Cytoskeletal Organization. *Ann Biomed Eng* 27(6):712–720.

6. Vigliotti A, Ronan W, Baaijens FPT, Deshpande VS (2016) A thermodynamically motivated model for stress-fiber reorganization. *Biomech Model Mechanobiol* 15(4):761–789.

7. Ujihara Y, et al. (2015) Computational studies on strain transmission from a collagen gel construct to a cell and its internal cytoskeletal filaments. *Comput Biol Med* 56:20–29.

Supporting Figure Legends

Figure S1: Modified computational model minimizes free energy ($\hat{g}_{tot} = \hat{g}_{cyto} + \hat{g}_{elas}$) based upon the boundary conditions to determine equilibrium cell strain. **A**) When the x_2 direction was constrained (strip uniaxial cases), stress fibers reached the same minimum free energy and cell strain in all directions ($E_{11}=E_{22}$). **B,C**) When the x_2 direction was free (uniaxial cases), stress fibers in x_2 (**C**) reached minimum free energy (**yellow diamond**) at a cell strain much lower than in x_1 (**B**).

Figure S2: Angular histograms of cell orientation for 10% uniaxial cyclic stretch (**A-C**) and 10% strip uniaxial cyclic stretch (**E-G**) at 0.5, 2, and 4 Hz after 72 hours. Each data point is representative of five independent experiments (except uniaxial 4 Hz, n=4), and expressed as the mean $\pm$ SD. Angular histograms of stress fiber orientation simulations for uniaxial (**D**) and strip uniaxial (**H**) conditions across our range of frequencies (**dotted** lines: 0.5 Hz, **dashed**: 2 Hz, **solid**: 4 Hz). *Insets* above the legend show circular histogram representations of these stress fibers.

Figure S3: The orientation of stress fibers within ten cells from each stretch condition (sixty total; symbols correspond with Figs. 2, 3) correlated strongly with the orientation of the entire cell. **A)** Orientation of the stress fibers (mean angle using stress fibers, MA^{SF}) versus tracing its boundary (MA^{cell}). **B)** Comparison of the strength of alignment of the cell using its stress fibers (mean vector length of stress

fibers, MVL^{SF}) versus the alignment of the cell using its boundary (MVL^{cell}).

Figure S4: Quantification of cell alignment. **A)** A representative 2D projection of F-actin stained adult rat cardiac fibroblasts taken from the core of the tissue. Scale bar, 200μm. **B)** Magnification of the boxed region in **(A)**, converted into a binary image. **C)** Vectors (dashed arrows represent subset of 400 vectors used) drawn from the centroid (dot) to the boundary of the cell were used to calculate the cell's strength of alignment (MVL^{cell}, ranging from 0, a circular cell, to 1, a highly aligned, spindly cell), and orientation (MA^{cell}) (thick black arrows). The top cell, which is longer and more highly aligned, has a higher MVL^{cell} (=0.85; MA^{cell}=13^o) than the bottom cell (MVL^{cell}=0.55; MA^{cell}=43^o). **D)** The mean vectors of all cells in **(A)** are saved and plotted. These vectors were used to then calculate each gel's overall mean vector length (MVL^{gel}, ranging from 0, cells randomly aligned, to 1, all cells strongly aligned in the same direction) and mean angle (MA^{gel}). In this image, the cells are aligned in the 0^o (x_1) direction with moderate strength.

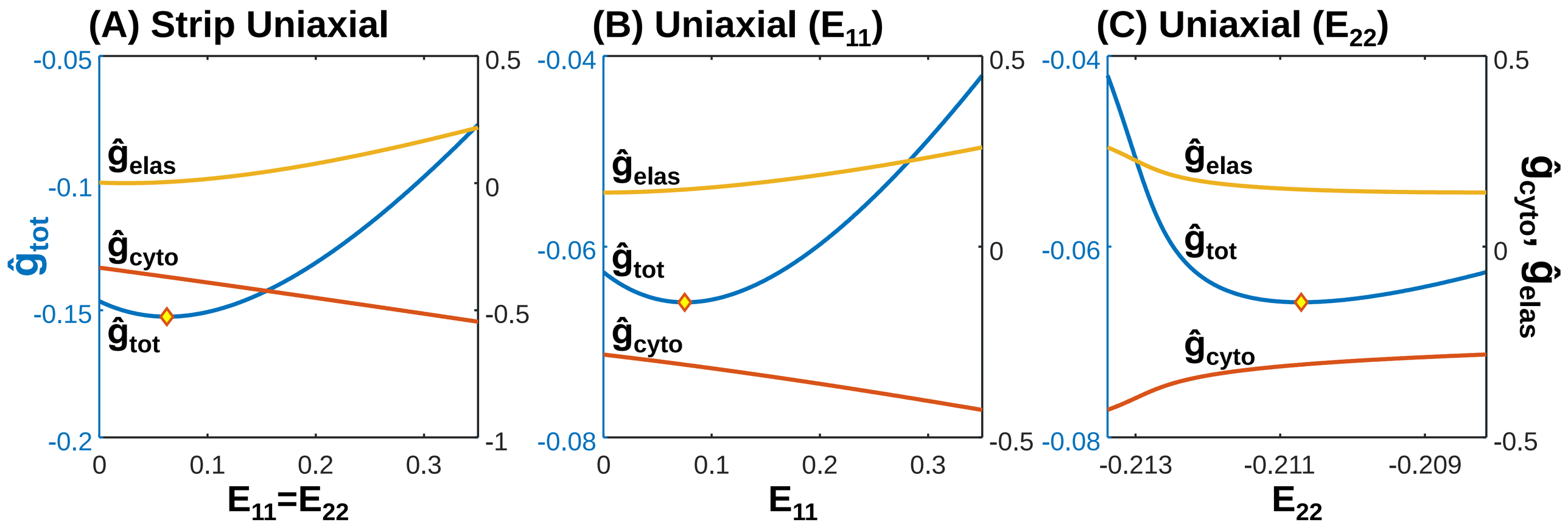
(A) Strip Uniaxial
(B) Uniaxial (E11)
(C) Uniaxial (E22)
ĝtot
ĝcyto, ĝelas
ĝelas
ĝcyto
ĝtot
E11=E22
E11
E22
-0.05
-0.1
-0.15
-0.2
-0.04
-0.06
-0.08
0.5
0
-0.5
-1
0
0.1
0.2
0.3
-0.213
-0.211
-0.209

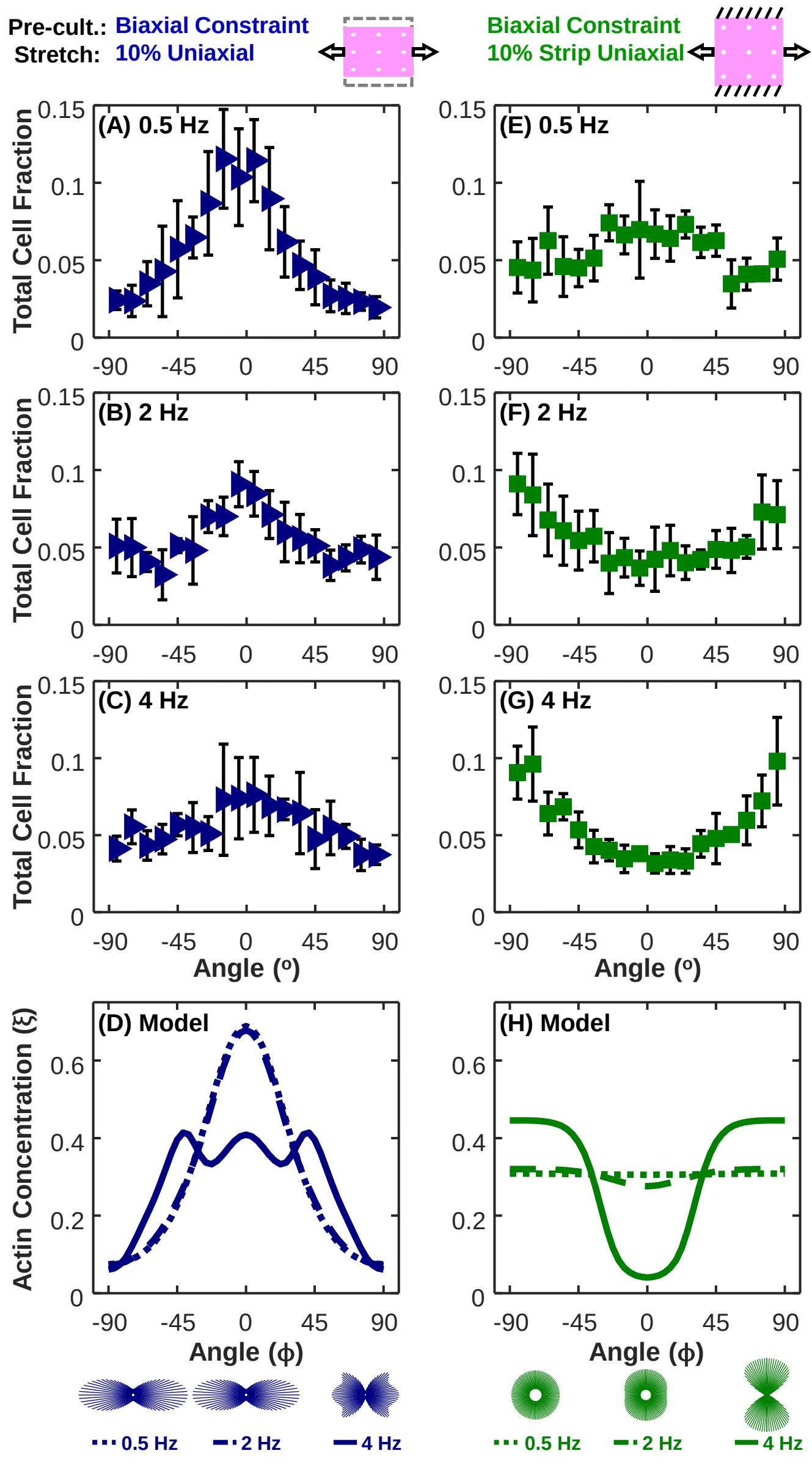
Pre-cult.: Biaxial Constraint
Stretch: 10% Uniaxial
Biaxial Constraint
10% Strip Uniaxial
(A) 0.5 Hz
(B) 2 Hz
(C) 4 Hz
(D) Model
(E) 0.5 Hz
(F) 2 Hz
(G) 4 Hz
(H) Model
Total Cell Fraction
Actin Concentration (ξ)
Angle (º)
Angle (ϕ)
0.5 Hz
2 Hz
4 Hz

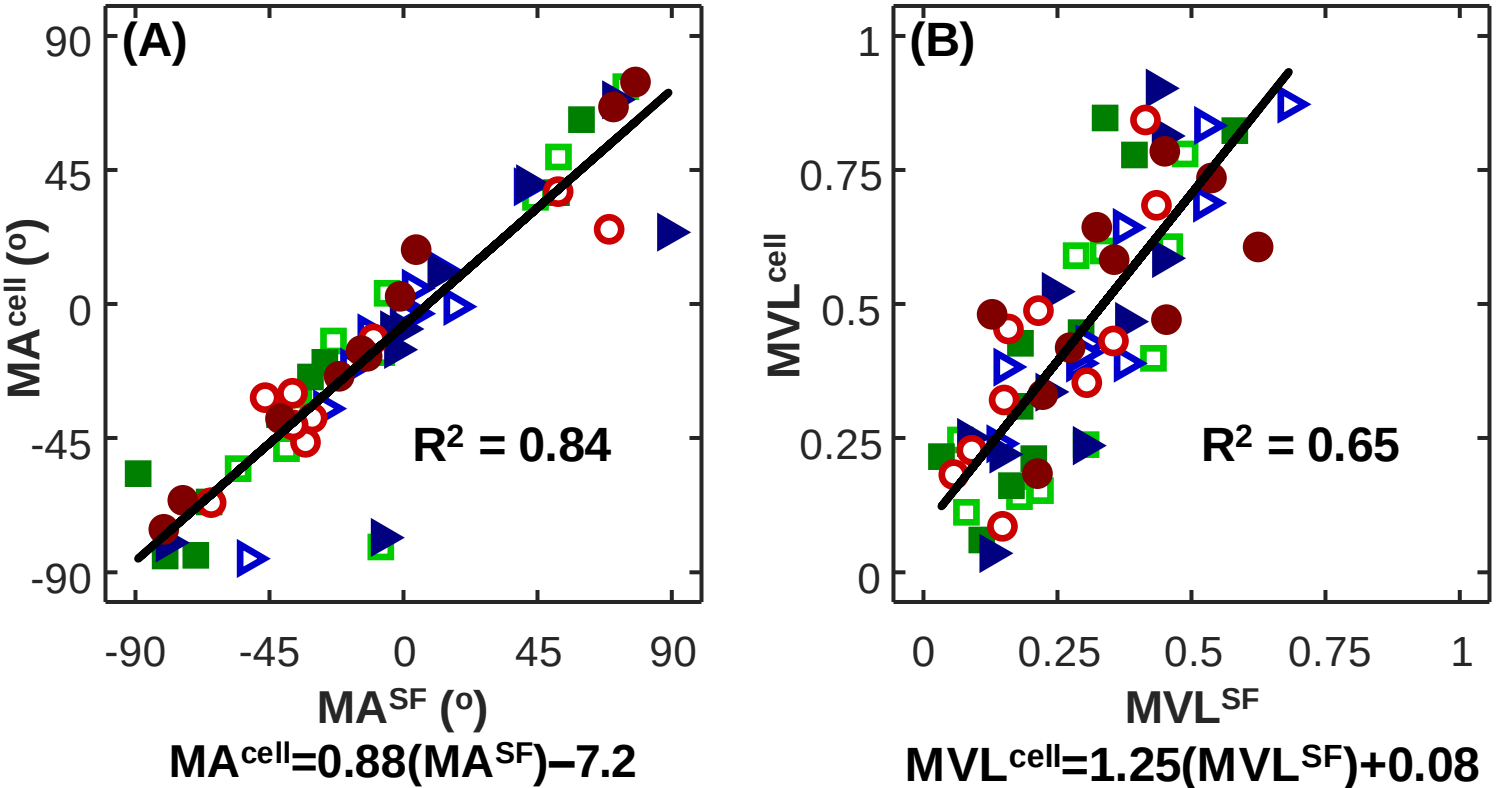
(A)
90
45
0
-45
-90
MA^cell (°)
-90
-45
0
45
90
MA^SF (°)
R² = 0.84
MA^cell=0.88(MA^SF)–7.2
(B)
1
0.75
0.5
0.25
0
MVL^cell
0
0.25
0.5
0.75
1
MVL^SF
R² = 0.65
MVL^cell=1.25(MVL^SF)+0.08

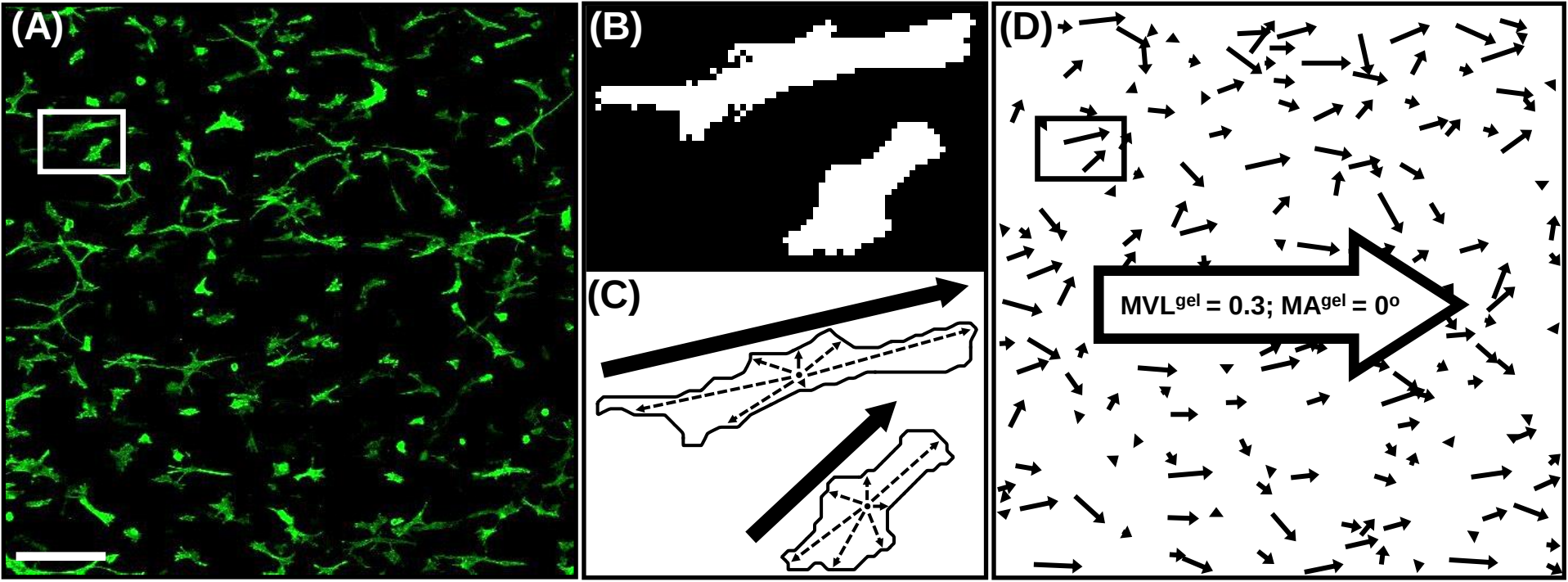
(A)
(B)
(C)
(D)
MVL^gel = 0.3; MA^gel = 0^o